# Electrochemical Studies of Capping Agent Adsorption Provide Insight into the Formation of Anisotropic Gold Nanocrystals

**Brook R. Danger, Donna Fan, J. P. Vivek,† and Ian J. Burgess***

Department of Chemistry, University of Saskatchewan, Saskatoon, Saskatchewan, S7N 5C9 Canada. †Present address: Department of Physics E19, Technical University of Munich, James-Franck-Strasse 1, 85748 Garching, Germany.

**ABSTRACT** The ability of the 4-dimethylaminopyridine (DMAP) to stabilize and control the formation of anisotropic gold nanocrystals produced *via* the borohydride reduction of gold(III) salts is reported here. Electrochemical measurements of DMAP electrosorption on different low-index single crystal and polycrystalline electrodes is provided and shows a propensity for DMAP to preferentially adsorb on {100} facets. Measuring the electrochemical potential during nanocrystal formation shows that experimental conditions can easily be manipulated so that the growth of nanoseeds occurs at potentials that support preferential DMAP adsorption on {100} surfaces giving rise to highly anisotropic nanocrystals (nanorods, bipyramids, and nanopods). Nanopods with nearly 50 nm arm lengths are shown to form and produce a surface plasmon mode that extends well into the near IR ($\lambda_{max} \approx 1350$ nm). Evidence is provided of the slow, partial reduction of tetrachloroaurate to a DMAP stabilized $Au^{I}$ species. Shape control is achieved simply by varying the length of time, $\tau$, that DMAP is allowed to partially reduce the $Au^{III}$ ions prior to the addition of the strong reducing agent, $NaBH_4$. Thus the role of DMAP in producing anisotropic particle shapes is shown to be multifunctional. A mechanism accounting for the dependence of particle shape on $\tau$ is provided.

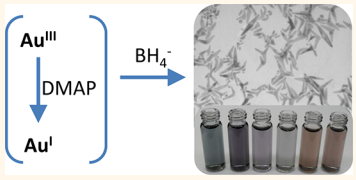


**KEYWORDS:** anisotropic nanocrystals · preferential adsorption · dimethylaminopyridine (DMAP) · nanopods · nanorods · bipyramids

Anisotropic metal nanoparticles, such as nanorods, nanoplates, nanoprisms, and nanopods have been, and continue to be, the subject of vigorous research activity most notably due to their tunable optical and electronic properties. The fabrication of these nanocrystals is an intriguing undertaking as it seemingly requires kinetically controlled synthesis conditions to overcome the tendency of nanocrystals to form thermodynamically favored, isotropic (quasi-spherical) structures.[1] Preferential overgrowth along one crystallographic direction is essential and there are now numerous reports of experimental conditions that lead to anisotropic metal nanoparticles.[2] Perhaps the most understood example is the formation of gold nanorods which follows a "seed-growth process"[3−5] whereby small (diameter less than 5 nm) quasi-spherical $Au^0$ seeds are added to a growth solution containing (1) a source of $Au^{III}$ ions (typically $AuCl_4^-$), (2) a mild reducing agent (usually ascorbic acid), and (3) a stabilizing surfactant such as cetyltrimethylammonium bromide, $C_{16}$TAB. Many aspects of the seed-growth method, such as the incomplete reduction of $Au^{III}$ to $Au^{I}$ by ascorbic acid[6] and the resulting disproportionation of $Au^{I}$, which is an autocatalyzed reaction occurring on the surface of $Au^0$ particles,[7−9] are now well understood. Mirkin's group has recently provided rules detailing how Ag and halide ions can define the shapes of gold nanoparticles produced in the seed-growth method.[10]

The synthesis of Pt multipodal nanocrystals (tripods, tetrapods, etc.) has been reported and high resolution transmission electron microscopy (TEM) results have shown that the nanocrystals arise from overgrowth along one family of crystallographic directions. For example, Xia and coworkers demonstrated that controlling the reduction kinetics of $Pt^{II}$ precursors could lead to different morphologies with fast reduction conditions producing spherical nanoparticles and slower rates yielding branched and one-dimensional nanostructures.[11−14] Multipods were found to contain between two to six arms resulting from preferential growth along the ⟨111⟩ directions of either single crystal or

* Address correspondence to ian.burgess@usask.ca.

Received for review October 6, 2012 and accepted November 27, 2012.

**Published online November 27, 2012**
**10.1021/nn304636m**

twinned seeds.[13] Manipulation of reduction conditions to favor either kinetic or thermodynamic control can be used to dictate the shape of Pt nanoparticles[15,16] and controlled secondary growth is paramount in generating nanocrystals of various anisotropic and branched shapes.[2,17−19]

The importance of Pt in catalysis and the need for engineered nanostructures with high surface areas enclosed by certain crystallographic facets[20] have driven much interest in Pt multipods but in recent years there have been increasing reports of branched Au metal nanoparticles.[21−28] Ortiz and Skrabalak[24] have indicated that common to all these reports are conditions providing a high concentration of adatoms that facilitate overgrowth and the formation of branched nanocrystals. This perspective is entirely reasonable if one considers only the growing seed and the required interplay between thermodynamic and kinetic control needed for the creation of anisotropic and/or branched nanocrystals. However, it does not account for the key role that can be played by preferential adsorption of capping/protecting agents on certain crystallographic facets of the growing nanocrystal. For example, it is widely believed that the evolution of penta-twinned (decahedral) seed crystals into gold nanorods occurs due to preferential $C_{16}$TAB adsorption and consequent retardation of $Au^0$ deposition on {100} surfaces.[29−31] It has also been reported that selective adsorption of citrate on {111} facets may be responsible for promoting the formation of nanobelts[32] and nanoplates.[33,34] Similarly, the presence of piperazine in HEPES buffer was shown by Xie *et al*. to be critical for forming highly branched Au metal nanocrystals, and the authors speculated this was caused by weak adsorption of the nitrogen heterocycle on {111} facets.[25] Huang and co-workers have used specific peptides for nanocrystal shape-control and argued that the different shapes produced are caused by peptide adsorption on high energy {110} facets.[18,35] Although many authors cite preferential capping adsorption in directing anisotropic nanocrystal growth, there are very few studies that attempt to fundamentally address this issue. This is primarily due to the intrinsic difficulty in measuring surfactant adsorption on growing, nanosized, structures in the presence of massive excesses of unbound ligand. We have recently shown that the use of millimeter-sized, single-crystal electrodes can provide quantitative information on the adsorption of nanoparticle-stabilizing surfactants.[36−40] In this report, we demonstrate that preferential adsorption of 4-dimethylaminopyridine (DMAP) on Au {100} leads to overgrowth of {111} facets and the formation of anisotropic metal nanoparticles including nanorods and nanopods. We also demonstrate that DMAP has a multifunctional role as it acts not only as a stabilizer but also is imperative in creating low rates of gold monomer deposition onto growing seed crystals.

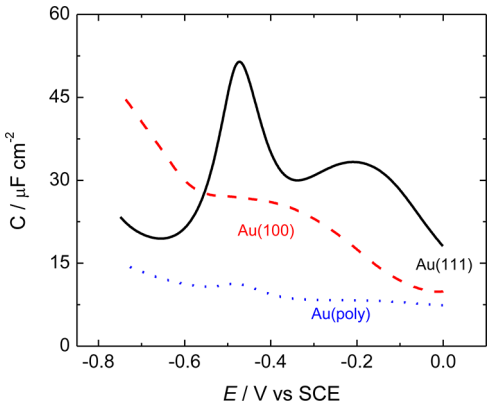


**Figure 1. Differential capacity (DC) curves recorded with a 5 mV/s negative-going potential sweep of various gold electrodes in the presence of 0.1 M DMAP and 0.05 M NaF supporting electrolyte. A 25 Hz, 5 mV (rms) sine wave was used as the ac perturbation. Au(111) (black line), Au(100) (dashed red line), Au(poly) (dotted blue line).**

Furthermore, we reveal how the shape of nanoparticles formed can easily be tuned to favor either spherical, one-dimensional (nanorods), or multidimensional (multipod) nanocrystals without fundamentally changing the reaction conditions.

## RESULTS AND DISCUSSION

**Electrochemistry.** The electrosorption of pyridine on gold has been shown by Lipkowski and co-workers to be highly dependent on surface crystallography.[41] However, unlike DMAP, pyridine is not a strong enough Lewis base to stabilize gold nanoparticles.[42] As previous studies[38] using polycrystalline gold revealed similar electrochemical behavior between DMAP and its parent compound, our starting rationale was that DMAP could serve as an excellent stabilizing ligand to promote the formation of anisotropic metal nanoparticles. Differential capacity curves for 0.10 M DMAP in the presence of 0.05 M NaF supporting electrolyte are shown in Figure 1 for millimeter sized Au(111), Au(100) and polycrystalline electrodes. Ignoring contributions from the diffuse part of the double layer, the measured capacity is determined by the inner layer of adsorbed molecules, $C = \varepsilon\varepsilon_0/d$, where $\varepsilon$ is the relative permittivity of the adsorbed layer, $\varepsilon_o$ is the vacuum permittivity, and $d$ is the separation between the metal electrode and the plane of closest approach of solvated electrolyte ions.[43] As organic molecules such as DMAP have relatively small values of $\varepsilon$ and are physically larger in size compared to water, a low measured capacity indicates molecular adsorption. The capacity curves in Figure 1 demonstrate that at potentials above −0.55 V the Au(111) surface has significantly less adsorbed DMAP compared to Au(100). Even lower capacities in this potential region for the polycrystalline Au electrode reveal that the DMAP coverage on higher energy surfaces such as {210} and {110} is very high. The differential capacity data imply that anisotropic

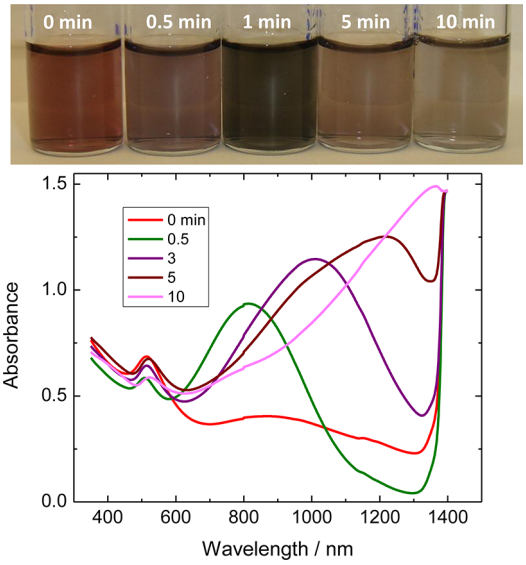


**Figure 2. (a) Color of colloidal gold solutions resulting from the addition of $NaBH_4$ to $HAuCl_4$-DMAP mixtures and (b) UV−vis−NIR optical spectra of the resulting dispersions. The time between mixing the $Au^{III}$ and DMAP and the addition of $NaBH_4$ ($\tau$) is indicated.**

nanocrystal formation should result from the slow growth of single-crystalline or twinned crystal gold seeds in the presence of a source of $Au^0$ atoms if DMAP is chosen as the stabilizing molecule. The difficulty arises in achieving suitable seed-growth conditions. The common method of using ascorbic acid to reduce $Au^{III}$ to form a growth solution of $Au^I$ for citrate stabilized gold seeds was attempted but in the presence of DMAP led to the formation of small Au nanoparticles embedded in polymerized ascorbic acid.[44]

Somewhat surprisingly, the direct addition of $NaBH_4$ to a 400:1 mixture of DMAP and $AuCl_4^-$ led to the formation of colored solutions (Figure 2a). This is unexpected as the strong reduction potential of $BH_4^-$ usually causes the immediate precipitation of $Au^0$ from solutions of gold salts unless strongly adsorbed capping agents such as thiols are present. The color of the solutions formed from the $BH_4^-$ reduction of tetrachloraurate in the presence of DMAP was found to be highly dependent on the time lapse, $\tau$, between the preparation of the $AuCl_4^-$-DMAP mixture and the addition of the reducing agent. Very small values of $\tau$ (less than 5 s) led to ruby red colors, intermediate values of $\tau$ provided green to purple colored solutions and longer values of $\tau$ (~10 min) provided brown to taupe colored solutions. The solutions were stable on the bench for hours to days depending on the final color with the smaller values of $\tau$ showing greater resistance to flocculation, whereas sedimentation of the colloidal dispersions was more pronounced in the taupe colored solutions. The varying optical appearances of the gold dispersions are indicative of the formation of different sizes and shapes of nanocrystals. Further information pertaining to the shape and size of

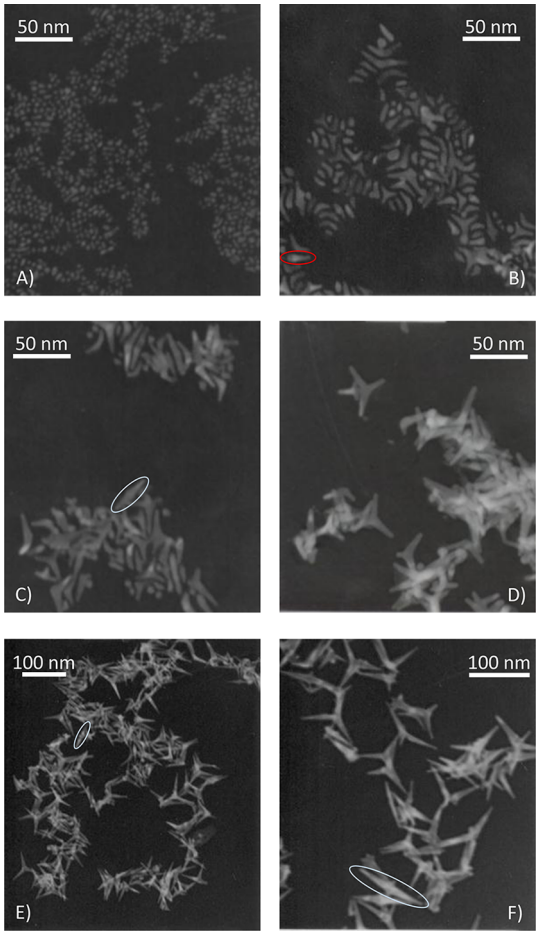


**Figure 3. Transmission electron micrographs of Au nanocrystals formed from the $NaBH_4$ reduction of $HAuCl_4$−DMAP mixtures as a function of $\tau$. (A) $\tau$ = 0 min, (B) $\tau$ = 0.5 min, (C) $\tau$ = 1 min, (D) $\tau$ = 3 min, (E) $\tau$ = 5 min, and (F) $\tau$ = 10 min. Red circle in image 3B highlights a nanorod with tapered extremities. Blue circles in images C, E, and F highlight elongated bipyramidal shapes.**

the nanocrystals can be extracted from the optical and near-infrared (NIR) extinction spectra shown in Figure 2b. A common peak is observed at ~525 nm which can be attributed to the surface dipole commonly observed for spherical gold nanoparticles and the transverse, dipolar modes of nanorods.[45] The position and intensity of this band varies only slightly with $\tau$ indicating subtle changes in the size and number density of the dimension that gives rise to this localized surface plasmon resonance.[45] More striking is the observation of a second extinction maximum that develops with increasing values of $\tau$. The spectra reveal that the higher wavelength peak further redshifts eventually extending well into the NIR for the taupe colored solutions. The observation of a second plasmon mode is highly indicative of the presence of anisotropic nanocrystals,[46,47] although extraction of the precise shape from the vis-NIR optical spectra would require detailed theoretical modeling.[48]

Conclusive evidence of the shapes formed is found from the TEM images shown in Figure 3. When $\tau$ = 0,

only small, quasi-spherical, particles are evident (see Figure 3A) and their average diameter is approximately 3−4 nm. The size and shape of these particles is quite consistent with the position of the surface plasmon maximum at 513 nm which is slightly blue-shifted compared to the value reported by Gandubert and Lennox for 6.2 ± 1 nm DMAP-stabilized nanoparticles.[42] Evidence of particle anisotropy is shown beginning with the images for $\tau = 0.5$ min (Figure 3B). Four major shapes dominate this TEM: (1) small nanoparticles of similar size to those in Figure 3A, (2) quasi-rodlike shapes, (3) boomerangs, and (4) tripods. The rods have aspect ratios in the range of 1.5−2.5 but sometimes appear to taper at their extremities rather than being perfectly cylindrical. Such a nanocrystal is enclosed in the red ellipse in Figure 3B. Figure 3 panels C−F indicate that larger values of $\tau$ provide smaller populations of quasi-spherical particles. Tripods become the dominant species and the length of the tripod arms increases with $\tau$. The branches of the nanopods in Figure 3C,D are relatively short (*ca.* 18−20 nm), whereas they are seen to extend up to 40−50 nm from the crystal core in Figure 3E,F. The majority "two-dimensional" species in Figure 3B appear largely cylindrical but the later panels reveal very few such structures. Instead, elongated bipyramids such as those enclosed in blue are the majority "linear" species. It is also interesting to note that the fraction of "boomerang" nanocrystals appears to diminish with increasing $\tau$, however, this may simply be that the increasing length of the nanopodal arms makes it hard to assign which arms belong to which core. For completeness we note that in some TEM images, T-shaped tripods and tetrahedral tetrapods could be observed as minority species (Supporting Information, Figure S-2). The tripodal shapes shown in Figure 3 have been shown by high resolution-TEM to be caused by the preferential growth along the ⟨111⟩ directions for both Au[25] and Pt[13,14,18,35] nanopods.

To correlate the synthesis conditions to the electrochemical data, the reaction was conducted in a simple two electrode cell where the open circuit potential (ocp) of a gold bead was measured *versus* a calomel reference electrode. The working electrode compartment of the cell initially contained 4 mL of 0.1 M DMAP and after the addition of 100 $\mu$L of 0.01MHAuCl$_4$ the system was left unperturbed for a variable amount of time, $\tau$. Subsequently, 100 $\mu$L of 0.01 M NaBH$_4$ was added, and the open circuit potential transient was recorded as a function of time. The ocp transients, with the time origin defined as the moment the NaBH$_4$ was added, are shown in Figure 4 for three different values of $\tau$. The region where preferential adsorption of DMAP on Au(100) and higher energy surfaces occurs is defined in Figure 4 by the shaded area. The potential transient for $\tau = 0$ initially falls below −0.6 V but rapidly increases as the borohydride is consumed by the reduction of gold ions and eventually stabilizes at a

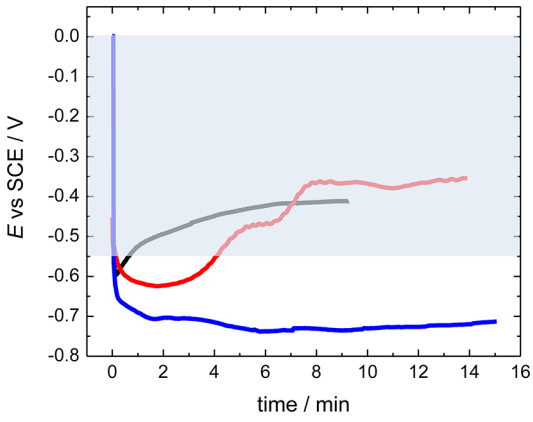


**Figure 4. Open-circuit potential measurements during the evolution of gold nanocrystals. The working electrode compartment of the cell initially contained 4 mL of 0.1 M DMAP and 100 $\mu$L of 0.01MHAuCl$_4$ that had been allowed to react for a controlled amount of time, $\tau$. The origin of the time axis corresponds to the moment that NaBH$_4$ was added to the cell. The shaded region defines the potential range where DMAP is preferentially adsorbed on Au {100} and Au(poly) facets. Black line ($\tau$ = 0 min), red line ($\tau$ = 5 min), blue line ($\tau$ = 60 min).**

value of *ca.* −0.4 V. The equivalent curve for $\tau = 60$ min shows that the potential falls further negative than −0.7 V after the addition of NaBH$_4$ and stays less than −0.7 V for more than 15 min. Following this transient for much longer times (see Supporting Information, Figure S-1) reveals that after nearly an hour, the potential increases which is concomitant with the observation of a very pale blue color in the solution. Eventually the solution became completely colorless and a dark precipitate was observed. The potential transient for $\tau$ = 5 min shows that the solution potential is sustained at −0.6 V for several minutes during which time the color of the solution slowly darkens from its initially pale yellow color. The solution further evolves into an intense brown-taupe color as the potential slowly rises into the regime where DMAP is preferentially adsorbed on {100} facets. Other potential transients show a consistent tendency for larger values of $\tau$ to result in longer persistence of negative solution potentials.

Cumulatively, Figures 1−3 demonstrate that the shape and size of DMAP stabilized gold nanostructures is determined by the value of $\tau$. It has been shown that size control can often be achieved by varying the rate of reduction[49] and the ratio of precursor to capping agent[50,51] both of which determine the relative rate of nucleation and growth. However, in the present case the reduction conditions are kept constant and it is the extent of the reaction between the DMAP and the $AuCl_4^-$ which is critical. As predicted from the electrochemical experiments, the presence of DMAP does indeed favor the formation of anisotropic nanostructures and can be rationalized by preferential growth on the less passivated {111} facets.

**Mechanism.** Engineered crystal design of anisotropic metal nanoparticles requires careful consideration of

the thermodynamic and kinetic factors that influence the nucleation and growth rates of the seed structures.[1] As the lowest energy surfaces of face-centered cubic (fcc) structures are {111} facets, single-crystals with octahedral and tetrahedral shapes fully bound by {111} planes should offer very low total energy shapes. However, these geometries are energetically taxed by the fact that they do not minimize the total surface area for a given number of atoms. Truncated octahedra (or cubooctahedra) are preferred in this regard, even though they present higher energy {100} surface facets, because of their near spherical shape.[1] Predicting the shape of seeds on a thermodynamic basis is complicated by crystal twinning which can further minimize the total surface energy of seeds at the cost of increased lattice strain. Crystal-twinning explains the formation of higher order seed shapes such as icosahedra and decahedra that can be built from tetrahedral subunits observed in theoretical[52,53] and experimental[29,54] studies. As the size of the seed particle increases, the energy cost from lattice strain begins to overwhelm the benefits of decreased surface area offered by crystal-twinning. Molecular dynamics simulations predict that increasing seed size leads to solid–solid phase transitions that favor the transformation of multiply twinned seeds into fcc truncated octahedra.[55] Although thermodynamic considerations can be used to predict the shape of the seed, other factors must be considered including the rate of precursor addition[56] and the influence of preferentially adsorbed capping molecules (see above). A mechanism to justify the results presented in this work must (1) address the probable structure of the seed crystals, (2) include a *proviso* about the rate of monomer (*i.e.*, $Au^0$) production for seed growth, and (3) account for the role of DMAP as a preferential capping agent.

The starting point for developing such a mechanism is the observation that the length of time between the addition of $HAuCl_4$ to the DMAP solution, prior to the introduction of the reducing agent, clearly plays a critical role in determining the shapes of the resulting nanoparticles. During this time the color of the $Au^{III}$–DMAP mixture fades from a very short-lived orange color (less than 1–2 s) to a pale yellow consistent with the formation of $[AuCl_2D_2]^+$ and $AuCl_3D$ complexes,[57,58] where $D$ = DMAP. Kinetic UV absorption traces (Supporting Information, Figures S-2 and S-3) show that the visible color of these solutions decreases with time. Pitteri and Bortoluzzi indicated that strong Lewis bases such as DMAP can partially reduce $Au^{III}$-pyridine complexes to $Au^I$ complexes[59] which is consistent with the slow fading of the color described above.

$$Au^{III}Cl_3D \xrightarrow{slow} [Au^{I}Cl_xD_{2-x}]^{1-x} \qquad x = 0, 1, \text{or } 2$$

On the basis of previous work on pyridine–$Au^I$ complexes, the most likely product of reduction is $Au^{I}D_2^+$ (*i.e.*, $x = 0$) or the dinuclear species $(Au^{I}D_2)_2^{2+}$.[60–62] Although $Au^I$ salts are usually colorless, owing to the absence of d–d orbital electronic transitions, computational studies on related compounds have shown that ligand-to-metal charge transfer can account for the persistence of the pale yellow color.[61] The slow transformation of $Au^{III}$ to the $Au^I$ species provides valuable insight on the importance of $\tau$ and the diversity of nanostructures formed. If the borohydride is preadded to the DMAP solution, the introduction of $HAuCl_4$ (*i.e.*, $\tau = 0$) results in a nucleation burst.[17,63] However, the borohydride exhaustively consumes all the available reducible gold ions preventing slow, further growth of these particles. This is evident in the potential transient which quickly increases to more positive values as the borohydride is nearly instantly depleted. It is important to note that these conditions support a rapid nucleation mechanism that produces a large number of small seeds with little to no subsequent monomer addition. Ostwald ripening of these very small seed particles leads to the color eventually changing to ruby red consistent with *ca.* 5–10 nm diameter DMAP stabilized nanoparticles.[42,64–67] At the opposite extreme, very large values of $\tau$ result in near complete transformation of $Au^{III}$ to $Au^I$ prior to the addition of the $NaBH_4$. The sustained negative potential in the transient indicates that the added borohydride is not immediately consumed in a redox reaction with the $Au^I$–DMAP complex. Given that for most ligands, the standard reduction potential for $Au^I + e^- \rightarrow Au^0$ is more positive than the reaction $Au^{III} + 3e^- \rightarrow Au^0$ it is likely that the former reduction process is kinetically very sluggish.[68] It is possible that the reduction of $Au^I$ to $Au^0$ proceeds through the autocatalytic disproportionation reaction,

$$3Au^+ \xrightarrow{Au^0} 2Au^0 + Au^{3+}$$

believed to be operative in the reduction of gold salts by ascorbic acid to yield nanorods.[69] We qualitatively tested this by monitoring the absorbance of $Au^{III}$ during the partial reduction process both in the presence and absence of metallic gold. If $Au^0$ catalyzes the disproportionation process one would expect the regeneration of $Au^{III}$ and the net result would be an apparently slower disappearance rate. Although differences are seen in the kinetic traces (Supporting Information, Figure S-3) they display the opposite trend to that expected for the autocatalytic disproportionation.

It is intermediate values of $\tau$ that are most intriguing as they lead to the coexistence of both $Au^{III}$ and $Au^I$ ions. These provide dual sources of $Au^0$ during nanoparticle formation and a two-stage growth process where the shape of the nanocrystals is easily manipulated.[70,71] Rapid reduction of $Au^{III}$ by borohydride yields small seeds, whose number density depends on the proportion of total gold that has yet to be

converted to $Au^{I}$ by DMAP reduction (*i.e.*, it depends on $\tau$). These seeds can either be single-crystalline tetrahedra, singly twinned tetrahedra (*i.e.*, octahedra), or multiply twinned tetrahedra (*e.g.*, decahedra) depending on the size and number of the seeds. Once formed, the slow borohydride reduction of $Au^{I}D_2^{+}$ provides a sustained feed of $Au^0$ monomers that grow the seed crystals into the nanocrystalline shapes shown in the TEM images (Figure 3). In this respect, the operative mechanism in this work provides similar results to those reported when competing reducers were employed to control the shape of Pt and PtCo nanocrystals.[72] Inspection of the potential transient for intermediate values of $\tau$ reveals that a significant portion of the quenching of borohydride lies in the potential range where DMAP is preferentially adsorbed on {100} facets. The slow rate of the $Au^0$ monomer generation provides conditions where the rate of adatom migration on the nanostructure is greater than the rate of $Au^0$ deposition and favors growth upon the most accessible facets of the seed. These slow growth conditions are conducive to more thermodynamic considerations such as the establishment of a lower DMAP adsorption coverage on {111} facets compared to the higher energy surfaces that are created during particle growth. This is a critical aspect in the formation of the anisotropic metal nanoparticles shown in Figure 3 and differs mechanistically from the rapid overgrowth conditions previously cited as a means to produce multipodal structures.[24] While the ability of adsorbed DMAP to direct growth explains the general observation of anisotropic particles it does not provide an immediate answer as to why these shapes are preferentially rod-like for smaller values of $\tau$ and multipodal for larger values of $\tau$. Differences in the structures of the seeds formed prior to the second stage of $Au^0$ deposition is likely and here the role of DMAP is to act as a protecting ligand rather than a director of anisotropic growth. $Au^0$ produced from the rapid reduction of $Au^{III}$ complexes likely nucleates into small tetrahedral building blocks that form either single-crystalline or a multitude of twinned seeds stabilized by DMAP adsorption. The degree of crystal twinning is determined by the size achieved by the seed crystals prior to secondary growth from the reduction of $Au^{I}D_2^{+}$. Small seed sizes that are dominant for small values of $\tau$ favor multiple twinning whereas larger $\tau$ yields the bigger seeds that favor singly twinned or single-crystalline structures. In the second stage of growth these seeds grow anisotropically along the ⟨111⟩ directions as the solution potential rises and sustains preferential DMAP adsorption on {100} facets. A proposed mechanistic scheme that accounts for the observed nanoparticle shapes is shown in Figure 5.

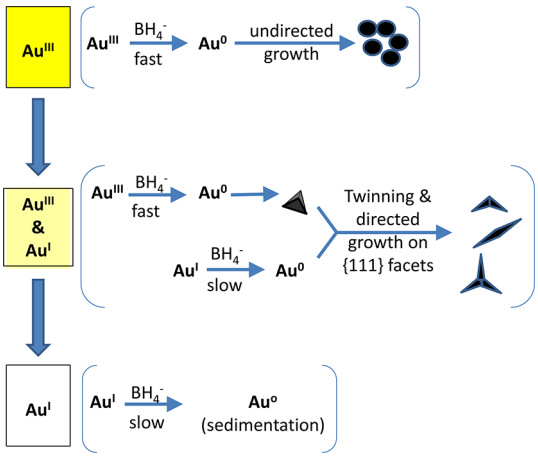


**Figure 5. Mechanistic scheme for the preparation of various sizes and shapes of DMAP stabilized anisotropic gold metal nanoparticles.**

## CONCLUSIONS

Different nanoparticle shapes, including spheres, rods, and long-armed branched nanopods have been produced from the reduction of $AuCl_4^-$ with $BH_4^-$ in a large excess of 4-dimethylaminopyridine (DMAP). Electrochemical measurements have provided both a rationale for the observation of anisotropic particles and important insight into the mechanism of seed-growth behavior. Key factors are the extent to which the slow reduction of $Au^{III}$ to $Au^{I}$ by DMAP occurs, the number density of $Au^0$ monomers formed in the initial reduction of $Au^{III}$ ions, and the electrochemical potential of the solution during secondary growth. It has been shown that slow, anisotropic, growth conditions occur on a variety of seed structures and a range of nanocrystalline shapes are eventually produced, including nanorods and tripods. It is evident that the formation of branched and anisotropic gold nanoparticles occurs under conditions of mixed thermodynamic, kinetic, and mass-transport control. Such conditions are quite familiar to electrochemists and this work illustrates how electrochemical measurements can offer valuable insight into nanoparticle seed and growth mechanisms. It also serves to highlight the need for a better understanding of the crystallographic dependent electrosorption of the capping agents commonly used as nanoparticle stabilizers.

## METHODS

$HAuCl_4$ (49% metals basis) was purchased from Alfa Aesar, whereas DMAP (99% purity) and NaF (99.99% purity) were obtained from Aldrich. All solutions were prepared using Millipore (18.2 MΩ cm) water. Aqueous solutions of 0.1 M DMAP, 0.01 M $HAuCl_4$, and 0.01 M $NaBH_4$ were prepared. The latter solution was kept in an ice bath at all times and freshly made after no more than 2 h. Nanocrystal synthesis was

achieved by adding 100 $\mu$L of $HAuCl_4$ to 4 mL of DMAP solution in a three dram vial. An orange color was noted immediately after addition, which quickly (less than 1−2 s) turned bright yellow. If borohydride was not added, this solution slowly turned faint yellow over the course of 10−20 min. Heating was found to accelerate this process although the solution did not go completely colorless even after several days. The addition of 100 $\mu$L of cold $NaBH_4$ led either to immediate coloring of the solution or the presence of a near transparent solution that slowly developed into a pronounced color depending on the value of $\tau$. Nanoparticle solutions were left to age for approximately 1 h before their optical-NIR spectra were measured using quartz cuvettes and a Cary 6000i (UV−vis−NIR) spectrometer or a Cary 100 (UV−vis only). Carbon film coated 200 mesh Cu TEM grids were prepared after similar aging times and images were collected using a Philips CM10 TEM with a plate film camera attachment. Electrochemical measurements were made using either a PAR173 or a HEKA 590 potentiostat and in-house software written in the LabVIEW environment. A two-electrode configuration was used with a gold bead serving as the working electrode and an SCE as the reference electrode. The SCE was separated from the working electrode compartment by a wetted stopcock to prevent chloride contamination. Details concerning differential capacity measurements have been provided elsewhere.[38] The methodology used to grow, orient, and cut gold single crystals has also been previously reported.[73] The gold electrodes were flame-annealed prior to electrochemical measurements. In the case of Au(100), the electrode was cycled at positive potentials to remove the well-known 5 × 20 thermal reconstruction,[74] and the strong adsorption of DMAP more than likely completely suppresses charge induced reconstruction at negative bias.

*Conflict of Interest:* The authors declare no competing financial interest.

*Acknowledgment.* This work was funded by a grant from the Natural Science and Engineering Research Council (NSERC) of Canada.

*Supporting Information Available:* Long time potential transient for $\tau$ = 60 min, UV−vis data of the DMAP−$Au^{III}$ complex, the kinetic traces of the reduction of $Au^{III}$ to $Au^{I}$ by DMAP, and an additional TEM showing atypical nanopod structures. This material is available free of charge *via* the Internet at http://pubs.acs.org.

## REFERENCES AND NOTES


1. Xia, Y.; Xiong; Yujie; Lim, B.; Skrabalak, S. E. Shape-Controlled Synthesis of Metal Nanocrystals: Simple Chemistry Meets Complex Physics?. *Angew. Chem., Int. Ed.* **2009**, *48*, 60–103.
2. Guerrero-Martinez, A.; Barbosa, S.; Pastoriza-Santos, I.; Liz-Marzan, L. M. Nanostars Shine Bright For You: Colloidal Synthesis, Properties and Applications of Branched Metallic Nanoparticles. *Curr. Opin. Colloid Interface Sci.* **2011**, *16*, 118–127.
3. Sau, T. K.; Murphy, C. J. Seeded High Yield Synthesis of Short Au Nanorods in Aqueous Solution. *Langmuir* **2004**, *20*, 6414–6420.
4. Busbee, B. D.; Obare, S. O.; Murphy, C. J. An Improved Synthesis of High-Aspect-Ratio Gold Nanorods. *Adv. Mater.* **2003**, *15*, 414–416.
5. Jana, N. R.; Gearheart, L.; Murphy, C. J. Wet Chemical Synthesis of High Aspect Ratio Cylindrical Gold Nanorods. *J. Phys. Chem. B* **2001**, *105*, 4065–4067.
6. Zumreoglu-Karan, B. A Rationale on the Role of Intermediate Au(III)−Vitamin C Complexation in the Production of Gold Nanoparticles. *J. Nanopart. Res.* **2009**, *11*, 1099–1105.
7. Jana, N. R.; Gearheart, L.; Murphy, C. J. Seed-Mediated Growth Approach for Shape-Controlled Synthesis of Spheroidal and Rod-like Gold Nanoparticles Using a Surfactant Template. *Adv. Mater.* **2001**, *13*, 1389–1393.
8. Gammons, C. H.; Yu, Y.; Williams-Jones, A. E. The Disproportionation of Gold(I) Chloride Complexes at 25 to 200 °C. *Geochim. Cosmochim. Acta* **1997**, *61*, 1971–1983.
9. Evans, D. H.; Lingane, J. J. Standard Potentials of the Couples Involving $AuBr_4^-$, $AuBr_2^-$, and Au in Bromide Media. *J. Electroanal. Chem. (1959−1966)* **1963**, *6*, 1–10.
10. Langille, M. R.; Personick, M. L.; Zhang, J.; Mirkin, C. A. Defining Rules for the Shape Evolution of Gold Nanoparticles. *J. Am. Chem. Soc.* **2012**, *134*, 14542–14554.
11. Lim, B.; Lu, X.; Jiang, M.; Camargo, P. H. C.; Cho, E. C.; Lee, E. P.; Xia, Y. Facile Synthesis of Highly Faceted Multioctahedral Pt Nanocrystals through Controlled Overgrowth. *Nano Lett.* **2008**, *8*, 4043–4047.
12. Herricks, T.; Chen, J.; Xia, Y. Polyol Synthesis of Platinum Nanoparticles: Control of Morphology with Sodium Nitrate. *Nano Lett.* **2004**, *4*, 2367–2371.
13. Chen, J.; Herricks, T.; Xia, Y. Polyol Synthesis of Platinum Nanostructures: Control of Morphology through the Manipulation of Reduction Kinetics. *Angew. Chem., Int. Ed.* **2005**, *44*, 2589–2592.
14. Chen, J.; Wiley, B. J.; Xia, Y. One-Dimensional Nanostructures of Metals: Large-scale Synthesis and Some Potential Applications. *Langmuir* **2007**, *23*, 4120–4129.
15. Teng, X.; Yang, H. Synthesis of Platinum Multipods: An Induced Anisotropic Growth. *Nano Lett.* **2005**, *5*, 885–891.
16. Gong, X.; Yang, Y.; Zhang, L.; Zou, C.; Cai, P.; Chen, G.; Huang, S. Controlled Synthesis of Pt Nanoparticles *via* Seeding Growth and Their Shape-Dependent Catalytic Activity. *J. Colloid Interface Sci.* **2010**, *352*, 379–385.
17. Mankin, M. N.; Mazumder, V.; Sun, S. One-Pot Synthesis of Pt Nanocubes and Nanopods *via* Burst Nucleation and Controlled Secondary Growth. *Chem. Mater.* **2010**, *23*, 132–136.
18. Ruan, L.; Chiu, C. Y.; Li, Y.; Huang, Y. Synthesis of Platinum Single-Twinned Right Bipyramid and {111}-Bipyramid through Targeted Control over Both Nucleation and Growth Using Specific Peptides. *Nano Lett.* **2011**, *11*, 3040–3046.
19. Lacroix, L. M.; Gatel, C.; Arenal, R.; Garcia, C. A.; Lachaize, S. A.; Blon, T.; Warot-Fonrose, B. A.; Snoeck, E.; Chaudret, B.; Viau, G. Tuning Complex Shapes in Platinum Nanoparticles: From Cubic Dendrites to Fivefold Stars. *Angew. Chem., Int. Ed.* **2012**, *51*, 4690–4694.
20. Vidal-Iglesias, F. J.; Aran-Asis, R. M.; Solla-Gullon, J.; Herrero, E.; Feliu, J. M. Electrochemical Characterization of Shape-Controlled Pt Nanoparticles in Different Supporting Electrolytes. *ACS Catal.* **2012**, *2*, 901–910.
21. Ali Umar, A.; Oyama, M. High-Yield Synthesis of Tetrahedral-Like Gold Nanotripods Using an Aqueous Binary Mixture of Cetyltrimethylammonium Bromide and Hexamethylenetetramine. *Cryst. Growth Des.* **2008**, *9*, 1146–1152.
22. Chen, S.; Wang, Z. L.; Ballato, J.; Foulger, S. H.; Carroll, D. L. Monopod, Bipod, Tripod, and Tetrapod Gold Nanocrystals. *J. Am. Chem. Soc.* **2003**, *125*, 16186–16187.
23. Lim, B.; Camargo, P. H. C.; Xia, Y. Mechanistic Study of the Synthesis of Au Nanotadpoles, Nanokites, and Microplates by Reducing Aqueous $HAuCl_4$ with Poly(vinyl pyrrolidone). *Langmuir* **2008**, *24*, 10437–10442.
24. Ortiz, N.; Skrabalak, S. E. Controlling the Growth Kinetics of Nanocrystals *via* Galvanic Replacement: Synthesis of Au Tetrapods and Star-Shaped Decahedra. *Cryst. Growth Des.* **2011**, *11*, 3545–3550.
25. Xie, J.; Lee, J. Y.; Wang, D. I. C. Seedless, Surfactantless, High-Yield Synthesis of Branched Gold Nanocrystals in HEPES Buffer Solution. *Chem. Mater.* **2007**, *19*, 2823–2830.
26. Hao, E.; Bailey, R. C.; Schatz, G. C.; Hupp, J. T.; Li, S. Synthesis and Optical Properties of "Branched" Gold Nanocrystals. *Nano Lett.* **2004**, *4*, 327–330.
27. Dinda, E.; Rashid, M.; Mandal, T. K. Amino Acid-Based Redox Active Amphiphiles to *in Situ* Synthesize Gold Nanostructures: From Sphere to Multipod. *Cryst. Growth Des.* **2010**, *10*, 2421–2433.
28. Li, J.; Wu, J.; Zhang, X.; Liu, Y.; Zhou, D.; Sun, H.; Zhang, H.; Yang, B. Controllable Synthesis of Stable Urchin-like Gold Nanoparticles Using Hydroquinone to Tune the Reactivity of Gold Chloride. *J. Phys. Chem. C* **2011**, *115*, 3630–3637.

29. Johnson, C. J.; Dujardin, E.; Davis, S. A.; Murphy, C. J.; Mann, S. Growth and Form of Gold Nanorods Prepared by Seed-Mediated, Surfactant-Directed Synthesis. *J. Mater. Chem.* **2002**, *12*, 1765–1770.
30. Nikoobakht, B.; El-Sayed, M. A. Preparation and Growth Mechanism of Gold Nanorods (NRs) Using Seed-Mediated Growth Method. *Chem. Mater.* **2003**, *15*, 1957–1962.
31. Nikoobakht, B.; El-Sayed, M. A. Evidence for Bilayer Assembly of Cationic Surfactants on the Surface of Gold Nanorods. *Langmuir* **2001**, *17*, 6368–6374.
32. Sun, Y.; Mayers, B.; Xia, Y. Transformation of Silver Nanospheres into Nanobelts and Triangular Nanoplates through a Thermal Process. *Nano Lett.* **2003**, *3*, 675–679.
33. Wang, L.; Chen, X.; Zhan, J.; Chai, Y.; Yang, C.; Xu, L.; Zhuang, W.; Jing, B. Synthesis of Gold Nano- and Microplates in Hexagonal Liquid Crystals. *J. Phys. Chem. B* **2005**, *109*, 3189–3194.
34. Kan, C.; Zhu, X.; Wang, G. Single-Crystalline Gold Microplates: Synthesis, Characterization, and Thermal Stability. *J. Phys. Chem. B* **2006**, *110*, 4651–4656.
35. Li, Y.; Huang, Y. Morphology-Controlled Synthesis of Platinum Nanocrystals with Specific Peptides. *Adv. Mater.* **2010**, *22*, 1921–1925.
36. Vivek, J. P.; Burgess, I. J. Insight into Chloride Induced Aggregation of DMAP-Monolayer Protected Gold Nanoparticles Using the Thermodynamics of Ideally Polarized Electrodes. *J. Phys. Chem. C* **2008**, *112*, 2872–2880.
37. Kunze, J.; Burgess, I.; Nichols, R.; Buess-Herman, C.; Lipkowski, J. Electrochemical Evaluation of Citrate Adsorption on Au(111) and the Stability of Citrate-Reduced Gold Colloids. *J. Electroanal. Chem.* **2007**, *599*, 147–159.
38. Barlow, B. C.; Burgess, I. J. Electrochemical Evaluation of 4-(Dimethylamino)pyridine Adsorption on Polycrystalline Gold. *Langmuir* **2006**, *23*, 1555–1563.
39. Vivek, J. P.; Burgess, I. J. Quaternary Ammonium Bromide Surfactant Adsorption on Low-Index Surfaces of Gold. 1. Au(111). *Langmuir* **2012**, *28*, 5031–5039.
40. Vivek, J. P.; Burgess, I. J. Quaternary Ammonium Bromide Surfactant Adsorption on Low-Index Surfaces of Gold. 2. Au(100) and the Role of Crystallographic-Dependent Adsorption in the Formation of Anisotropic Nanoparticles. *Langmuir* **2012**, *28*, 5040–5047.
41. Lipkowski, J.; Stolberg, L. Molecular Adsorption at Gold and Silver Electrodes. In *Adsorption of Molecules at Metal Electrodes*; Jacek Lipkowski, P. N. R., Ed.; VCH: New York, 1992; pp 171−238.
42. Gandubert, V. J.; Lennox, R. B. Assessment of 4--(Dimethylamino)pyridine as a Capping Agent for Gold Nanoparticles. *Langmuir* **2005**, *21*, 6532–6539.
43. Delahay, P. *Double Layer and Electrode Kinetics*; Interscience Publishing: Hoboken, NJ, 1966.
44. Markham, R. G.; Elders, G. W.; Webb, R. C. Ascorbic Acid Derivatives and a Method for Their Preparation. EP0129343, Dec 27, 1984.
45. Eustis, S.; El-Sayed, M. A. Why Gold Nanoparticles are More Precious than Pretty Gold: Noble Metal Surface Plasmon Resonance and Its Enhancement of the Radiative and Nonradiative Properties of Nanocrystals of Different Shapes. *Chem. Soc. Rev.* **2006**, *35*, 209–217.
46. Hu, M.; Chen, J.; Li, Z. Y.; Au, L.; Hartland, G. V.; Li, X.; Marquez, M.; Xia, Y. Gold Nanostructures: Engineering Their Plasmonic Properties for Biomedical Applications. *Chem. Soc. Rev.* **2006**, *35*, 1084–1094.
47. Perez-Juste, J.; Pastoriza-Santos, I.; Liz-Marzan, L. M.; Mulvaney, P. Gold Nanorods: Synthesis, Characterization and Applications. *Coord. Chem. Rev.* **2005**, *249*, 1870–1901.
48. Yang, W. H.; Schatz, G. C.; Van Duyne, R. P. Discrete Dipole Approximation for Calculating Extinction and Raman Intensities for Small Particles with Arbitrary Shapes. *J. Chem. Phys.* **1995**, *103*, 869–875.
49. Okitsu, K.; Yue, A.; Tanabe, S.; Matsumoto, H.; Yobiko, Y. Formation of Colloidal Gold Nanoparticles in an Ultrasonic Field: Control of Rate of Gold(III) Reduction and Size of Formed Gold Particles. *Langmuir* **2001**, *17*, 7717–7720.
50. Leff, D. V.; Ohara, P. C.; Heath, J. R.; Gelbart, W. M. Thermodynamic Control of Gold Nanocrystal Size: Experiment and Theory. *J. Phys. Chem.* **1995**, *99*, 7036–7041.
51. Hostetler, M. J.; Wingate, J. E.; Zhong, C. J.; Harris, J. E.; Vachet, R. W.; Clark, M. R.; Londono, J. D.; Green, S. J.; Stokes, J. J.; Wignall, G. D.; *et al.* Alkanethiolate Gold Cluster Molecules with Core Diameters from 1.5 to 5.2 nm: Core and Monolayer Properties as a Function of Core Size. *Langmuir* **1998**, *14*, 17–30.
52. Saika-Voivod, I.; Poon, L.; Bowles, R. K. The Role of FCC Tetrahedral Subunits in the Phase Behavior of Medium Sized Lennard-Jones Clusters. *J. Chem. Phys.* **2010**, *133*, 074503–074507.
53. Asuquo, C. C.; Bowles, R. K. Molecular Dynamics Simulations of Competitive Freezing in Gold Nanoclusters. *J. Phys. Chem. C* **2012**, *116*, 14619–14626.
54. Harada, M.; Kamigaito, Y. Nucleation and Aggregative Growth Process of Platinum Nanoparticles Studied by *in Situ* Quick XAFS Spectroscopy. *Langmuir* **2011**, *28*, 2415–2428.
55. Baletto, F.; Mottet, C.; Ferrando, R. Microscopic Mechanisms of the Growth of Metastable Silver Icosahedra. *Phys. Rev. B* **2001**, *63*, 155408.
56. Humphrey, S. M.; Grass, M. E.; Habas, S. E.; Niesz, K.; Somorjai, G. A.; Tilley, T. D. Rhodium Nanoparticles from Cluster Seeds: Control of Size and Shape by Precursor Addition Rate. *Nano Lett.* **2007**, *7*, 785–790.
57. Bourosh, P.; Bologa, O.; Simonov, Y.; Gerbeleu, N.; Lipkowski, J.; Gdaniec, M. Synthesis and Structure of Products of Interaction of $HAuCl_4$ with $H_2DMG$ and Pyridine. *Inorg. Chim. Acta* **2007**, *360*, 3250–3254.
58. Li, J.; Hu, J.; Gu, Y.; Mei, F.; Li, T.; Li, G. Catalytic Activities and Properties of Au(III)/Schiff-Base Complexes in Methanol Oxidative Carbonylation. *J. Mol. Catal. A: Chem.* **2011**, *340*, 53–59.
59. Pitteri, B.; Bortoluzzi, M. Displacement of Neutral Nitrogen Donors by Chloride in $AuCl_3$(am) (am = Pyridines and Amines): Kinetics and DFT Calculations Show the Effects of Basicity and $\pi$−Acceptor Ability. *Eur. J. Inorg. Chem.* **2007**, *2007*, 4456–4461.
60. Chiou, J. Y. Z.; Luo, S. C.; You, W. C.; Bhattacharyya, A.; Vasam, C. S.; Huang, C. H.; Lin, I. J. B. Gold(I) Complexes of *N*-Heterocyclic Carbenes and Pyridines. *Eur. J. Inorg. Chem.* **2009**, *2009*, 1950–1959.
61. Lin, J. C. Y.; Tang, S. S.; Vasam, C. S.; You, W. C.; Ho, T. W.; Huang, C. H.; Sun, B. J.; Huang, C. Y.; Lee, C. S.; Hwang, W. S.; *et al.* Structural, Photophysical, and Catalytic Properties of Au(I) Complexes with 4-Substituted Pyridines. *Inorg. Chem.* **2008**, *47*, 2543–2551.
62. Ovejero, P.; Mayoral, M. a. J.; Cano, M.; Lagunas, M. a. C. Luminescence of Neutral and Ionic Gold(I) Complexes Containing Pyrazole or Pyrazolate-Type Ligands. *J. Organomet. Chem.* **2007**, *692*, 1690–1697.
63. LaMer, V. K.; Dinegar, R. H. Theory, Production and Mechanism of Formation of Monodispersed Hydrosols. *J. Am. Chem. Soc.* **1950**, *72*, 4847–4854.
64. Rucareanu, S.; Gandubert, V. J.; Lennox, R. B. 4-(*N*,*N*-Dimethylamino)pyridine-Protected Au Nanoparticles: Versatile Precursors for Water- and Organic-Soluble Gold Nanoparticles. *Chem. Mater.* **2006**, *18*, 4674–4680.
65. Gittins, D. I.; Caruso, F. Spontaneous Phase Transfer of Nanoparticulate Metals from Organic to *Aqueous* Media. *Angew. Chem., Int. Ed.* **2001**, *40*, 3001–3004.
66. Gittins, D. I.; Susha, A. S.; Schoeler, B.; Caruso, F. Dense Nanoparticulate Thin Films *via* Gold Nanoparticle Self-Assembly. *Adv. Mater.* **2002**, *14*, 508–512.
67. Griffin, F.; Fitzmaurice, D. Preparation and Thermally Promoted Ripening of Water-Soluble Gold Nanoparticles Stabilized by Weakly Physisorbed Ligands. *Langmuir* **2007**, *23*, 10262–10271.
68. Kohl, P. A. Electrodeposition of Gold. In *Modern Electroplating*; John Wiley & Sons, Inc.: 2010; pp 115−130.
69. Edgar, J. A.; McDonagh, A. M.; Cortie, M. B. Formation of Gold Nanorods by a Stochastic "Popcorn" Mechanism. *ACS Nano* **2012**, *6*, 1116–1125.

70. Zheng, H.; Smith, R. K.; Jun, Y. w.; Kisielowski, C.; Dahmen, U.; Alivisatos, A. P. Observation of Single Colloidal Platinum Nanocrystal Growth Trajectories. *Science* **2009**, *324*, 1309–1312.
71. Langille, M. R.; Zhang, J.; Personick, M. L.; Li, S.; Mirkin, C. A. Stepwise Evolution of Spherical Seeds into 20-Fold Twinned Icosahedra. *Science* **2012**, *337*, 954–957.
72. Lim, S. I.; Varon, M.; Ojea-Jimenez, I.; Arbiol, J.; Puntes, V. Exploring the Limitations of the Use of Competing Reducers to Control the Morphology and Composition of Pt and PtCo Nanocrystals. *Chem. Mater.* **2010**, *22*, 4495–4504.
73. Vivek, J. P.; Burgess, I. J. Adsorption of a Quaternary Ammonium Surfactant on Au(100). *J. Electroanal. Chem.* **2010**, *649*, 16–22.
74. Kolb, D. M. Reconstruction Phenomena at Metal−Electrolyte Interfaces. *Prog. Surf. Sci.* **1996**, *51*, 109–173.